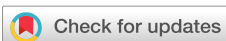


RESEARCH ARTICLE | MARCH 14 2024

# Performance measurements for indoor photovoltaic devices: Classification of a novel light source

D. E. Parsons   ; G. Koutsourakis  ; J. C. Blakesley 

APL Energy 2, 016110 (2024)

<https://doi.org/10.1063/5.0186028>View  
OnlineExport  
Citation

## Articles You May Be Interested In

Importance of spectrally invariant broadband attenuation of light in indoor photovoltaic characterization

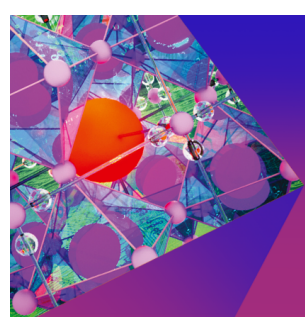
APL Energy (September 2023)

Thermodynamic principles for optimizing multi-junction photovoltaics—Exemplified for perovskite-based indoor photovoltaics

APL Energy (July 2025)

Chromaticity manipulation of indoor photovoltaic cells

Appl. Phys. Lett. (January 2021)



**APL Energy**  
Special Topics  
Open for Submissions

**Submit Today**

# Performance measurements for indoor photovoltaic devices: Classification of a novel light source

Cite as: APL Energy 2, 016110 (2024); doi: [10.1063/5.0186028](https://doi.org/10.1063/5.0186028)

Submitted: 3 November 2023 • Accepted: 20 February 2024 •

Published Online: 14 March 2024



[View Online](#)



[Export Citation](#)



[CrossMark](#)

D. E. Parsons,<sup>a)</sup> G. Koutsourakis, and J. C. Blakesley

## AFFILIATIONS

National Physical Laboratory, Hampton Road, Teddington TW11 OLW, United Kingdom

<sup>a)</sup>Author to whom correspondence should be addressed: [daniel.parsons@npl.co.uk](mailto:daniel.parsons@npl.co.uk)

## ABSTRACT

There is an increasing interest in using indoor photovoltaic (IPV) devices to power Internet of Things applications, low power communications, and indoor environmental sensing. For the commercialization of IPV technologies, device performance measurements need to conform to the relevant standardized specifications. We present a novel IPV device measurement system that incorporates digital light processing (DLP) to deliver a spectrally invariant light source at all required illuminance levels, as specified by the indoor standard testing conditions in IEC TS 62607-7-2:2023. We evaluated the DLP system according to requirements for spectral coincidence, temporal stability, and non-uniformity at the sample plane. We demonstrate the measurements to define the classification status of the system and the unique benefits of the DLP system that allow a stable spectral profile and high levels of uniformity across all illuminance levels. This is the first reported measurement system for IPV device testing based on DLP technology, and the classification methodology of this work can be used as an example for the classification of indoor light simulators in laboratory environments based on the latest IEC TS 62607-7-2:2023.

© 2024 Author(s). All article content, except where otherwise noted, is licensed under a Creative Commons Attribution (CC BY) license (<http://creativecommons.org/licenses/by/4.0/>). <https://doi.org/10.1063/5.0186028>

## I. INTRODUCTION

Indoor light harvesting has been identified as an energy source that has the potential to power the Internet of Things (IoT) ecosystem, including, among others, environmental sensors and communications devices.<sup>1</sup> Crystalline silicon (Si) photovoltaic (PV) devices commonly used outdoors are not ideal for indoor use; their bandgap (1.12 eV) is suboptimal for common indoor light sources that mainly emit in the visible range, and low shunt resistance causes significant losses in low light conditions.<sup>2</sup> Although in the past, low cost amorphous silicon (a-Si) PV devices dominated indoor applications, several different PV technologies have emerged for indoor light harvesting, demonstrating high efficiencies, potentially low costs, and sustainable manufacturing.<sup>3</sup> Organic PV (OPV) devices have already been commercialized and used for IPV applications, while their scalability potential has been well investigated.<sup>4</sup> Dye-sensitized solar cells can be designed so that they are optimized for the indoor spectrum, achieving high efficiencies under low light conditions.<sup>5</sup> Perovskite solar cell technologies are also being demonstrated under

indoor light conditions, achieving high efficiencies due to their optimized bandgap and structure for common indoor spectra and low light conditions.<sup>6,7</sup> Even past materials such as selenium are revisited for evaluation under indoor conditions, achieving respectable efficiencies.<sup>8</sup>

Although high efficiencies are being reported under indoor conditions for various technologies, it has been quite common that different labs use different conditions for power and efficiency measurements. This includes the use of different light sources, such as white LEDs with different color temperatures or fluorescent or other lamps, and different light levels, with values varying from 200 lx up to 2000 lx.<sup>7,9,10</sup> This makes the comparison of reported efficiencies of different technologies challenging, if not impossible, highlighting the need to define Indoor Standard Testing Conditions (ISTCs). Until recently, there was also a lack of established independent measurements offered by test labs in this area due to the lack of specified indoor conditions for testing. Responding to this need, these conditions are now defined in IEC TS 62607-7-2:2023 (Nanomanufacturing-Key control characteristics-Part 7-2:

**TABLE I.** The three illuminance levels, temperature, and spectrum specifications for performance testing of IPV devices at ISTC.<sup>11</sup> Testing at different illuminance levels ensures that device performance is tested within the common range of light levels in indoor environments.

Illuminance (lx)	Irradiance with LED-B4 spectrum (mW m <sup>-2</sup> )	Irradiance with FL10 spectrum (mW m <sup>-2</sup> )
1000	3132	3076
200	626	615
50	157	154
Temperature (°C)	25	
Spectrum	CIE B4-LED reference spectrum (white LED)	CIE FL10 reference spectrum (fluorescence lamp)

Nano-enabled photovoltaics–Device evaluation method for indoor light) and are discussed in Sec. II of this work.<sup>11</sup> This will allow measurements and appropriate comparisons of different technologies and architectures of indoor PV devices, under the same ISTC conditions.

The implementation of a measurement system that can deliver indoor PV device measurements at ISTC conditions is not trivial. IEC TS 62607-7-2:2023 requires measurements at three different light levels (50 lx, 200 lx, and 1000 lx) to ensure that IPV device linearity features are considered. It has already been reported that changing the light intensity without changing the spectral profile is non-trivial and can lead to different uncertainties, depending on the attenuation method used.<sup>12</sup> This is a challenging feature on top of requirements regarding spatial uniformity and stability of light sources.

In this work, we present the development and classification of a digital light processing (DLP) indoor light simulation system for performance testing of indoor PV devices at ISTC conditions. The system was specifically developed to be compliant with IEC TS 62607-7-2:2023 and is based on a digital micromirror device (DMD),<sup>13</sup> as presented in the following sections. The usefulness of such DLP systems for the metrology of PV devices has already been demonstrated in recent work. We have introduced high resolution linearity measurements of PV devices using a DLP system<sup>14</sup> and achieved megapixel resolution current mapping with such a system using compressed sensing methods.<sup>15</sup> DLP

systems have also been reported for spectral response measurements, where they can increase measurement speed and signal-to-noise ratio.<sup>16</sup>

Here, we have combined our DLP system with a white LED light source to develop the first DMD based indoor light simulator specifically for testing IPV devices. We present the requirements for such a system in order to achieve ISTC conditions and the process of classifying our system regarding spectral coincidence, stability, and irradiance uniformity at the sample plane. Results show that the DLP system can achieve an A rating for a 4 × 4 cm<sup>2</sup> area and a B rating for a 7 × 7 cm<sup>2</sup> area. Such a system can deliver accurate power ratings for IPV devices but also potentially indoor reference cell calibration. The classification methodology in this work can also be used as an example for research laboratories or indoor PV manufacturers to be aware of the requirements of their light sources and be able to classify their indoor testing systems before measurements. This will lead to harmonized reporting of efficiencies in the literature and meaningful comparisons between technologies. More importantly, indoor PV products on the market will have a common reference for comparison and will be able to reliably report products in their datasheets.

## II. INDOOR STANDARD TESTING CONDITIONS

IEC TS 62607-7-2 ED1 sets out the requirements for power and efficiency measurements of PV devices under indoor conditions.<sup>11</sup> The principle of the specification dictates that all devices of any type must be measured under the same illumination conditions (illuminance, spectrum, and temperature). Measurement of IPV device efficiency or power requires a light source, a calibrated source meter for measuring power output, and a calibrated reference device against which IPV devices are compared. The accuracy and quality of all three of these components are crucial for accurate measurements. In this work, however, we focus on the light source of such measurements. These specifications include the classification requirements for light sources that simulate indoor conditions, as well as specifications for measurement conditions such as temperature requirements, traceability, and spectral mismatch corrections. Table I shows the ISTC specification for testing IPV devices. The difference between irradiance and illuminance should be noted for the discussions in this work; irradiance is the radiant flux received by a specific area, and its units are W/m<sup>2</sup>, while illuminance is the total luminous flux per unit area, with its units being lux (lx) or lumens (lm)/m<sup>2</sup>.<sup>17</sup> Luminous flux refers to the radiant flux, wavelength-weighted by the luminosity function to correlate with human brightness perception.

**TABLE II.** Specifications for light source classification for IPV measurements.<sup>11</sup> Spectral coincidence is a parameter determined by the mismatch between the used light source spectrum and the CIE spectrum.

Class	SA	A	B	C
Spectral coincidence	0.95–1.05	0.75–1.25	0.6–1.4	0.4–2.0
Spatial non-uniformity	within ±2%	within ±2%	within ±5%	within ±10%
Temporal stability	within ±0.5%	within ±0.5%	within ±2%	within ±10%

Testing at different illuminance levels ensures that device performance is reported at different illuminance levels within the common range of indoor environments. This is important since the PV devices can demonstrate very non-linear behavior at such low light levels.<sup>18,19</sup> Such non-linearities will affect the power and, hence, the efficiencies of devices in low light conditions. Current-voltage (I-V) characteristic curves are to be acquired at each of these illuminance levels and the methods described in IEC 60904-1:2020 regarding I-V measurement acquisition still stand.<sup>20</sup> For indoor PV testing, since the indoor light can be highly diffuse, there is no requirement for the light source to be collimated, so light sources can be pseudo-collimated, pseudo-isotropic, or anything in between. Nevertheless, the angular distribution of the light source impacts measured values and uncertainties since each device will have a unique angular response. Due to such angular effects, lower uncertainties are expected with more collimated light sources.

The light source should be as close as possible to a defined standard reference spectrum. ISTC specifications provide two options for reference spectrum: the CIE B4-LED reference spectrum, which represents LED illumination, or the CIE FL10 reference spectrum, which represents illumination by a fluorescent lamp, as defined in CIE 015:2018.<sup>11</sup> An LED is used in this work, so the CIE B4-LED reference spectrum is considered. This is a modeled spectrum, so it will be difficult for an existing LED light source to exactly match this spectrum. Hence, all I-V measurements should be corrected to this spectrum by applying a spectral mismatch correction; the spectral response of the PV device under test, the spectral response of the reference, and the spectral profile of the light source, need to be known. Under the irradiance conditions required for indoor PV, the 25 °C temperature requirement is achieved by heating, rather than cooling, the sample.

IEC TS 62607-7-2 describes the criteria for classifying light sources for IPV testing according to three characteristics: spectral coincidence, spatial non-uniformity, and temporal stability. These are shown in Table II. These criteria echo the approach of IEC 60904-9 for classifying solar simulators.<sup>21</sup> Light sources are classified from SA to C for each characteristic, with SA representing the class with the greatest accuracy. Note, however, that a good light source is necessary but not sufficient for good accuracy; calibrated reference devices, instruments and suitable procedures are also important.

### III. DLP SYSTEM DESIGN FOR ISTC TESTING

Our system has been designed to project pseudo-collimated light onto a measurement plane using a white LED light source coupled with a digital micromirror device (DMD). A DMD is an array of micromirrors that can be programmatically controlled to “on” and “off” pixels to produce user-defined patterns.<sup>13</sup> A light source is directed through the device’s coupling optics, which collimate the incoming light onto these arrays of micromirrors. The micromirrors are individually controlled by an electronic control card. Pixels that are defined as “on” reflect the incoming light onto a set of projection optics directed toward the area of interest. This enables the use of the DMD to reduce the illuminance level at a sample plane by controlling the number of pixels we turn “on” as opposed to controlling the current through the LED. As the reflectivity of the DMD micromirrors is uniform across the visible spectrum, the spectrum of the projected light source will not change when the pattern changes. Methods of using optical attenuation to reduce the light intensity have been reported, but spectral deviations were also observed.<sup>12</sup>

A schematic of our DLP system for ISTC testing of PV devices is presented in Fig. 1. The system is based on a Cree CXA2 5000 K CRI 70 white LED, coupled to the projection module of a Vialux V-7001 DMD development kit. This LED was chosen as it had a similar spectrum to the CIE B4-LED reference spectrum, and its luminous flux of 2002 lumens enabled us to achieve illuminances of over 1000 lx at our desired working distance. An additional 50 mm lens (100 mm focal length) is placed at the output of the projection optics to ensure the projection is maintained out of focus on the sample plane and to improve its collimation. The projection at the sample plane is intentionally “out of focus,” so that a smooth and uniform light field is achieved. The beam goes through three baffles to reduce stray light toward the sample, then a flat front coated mirror at a 45° angle guides the beam to the sample plane so samples can be placed horizontally on the measurement platform. The platform is placed on top of an x-y stage to enable measurements of spatial non-uniformities within the region of interest (ROI). A Keithley 2401 source meter is used for I-V measurements. The sample platform includes temperature control and feedback, with additional temperature control of the enclosure space, to keep both the sample platform and the enclosure space at 25 °C. The DMD used is an array of 1024 × 768 micromirrors that reflect the input light from the coupling optics onto the integrated projection optics.

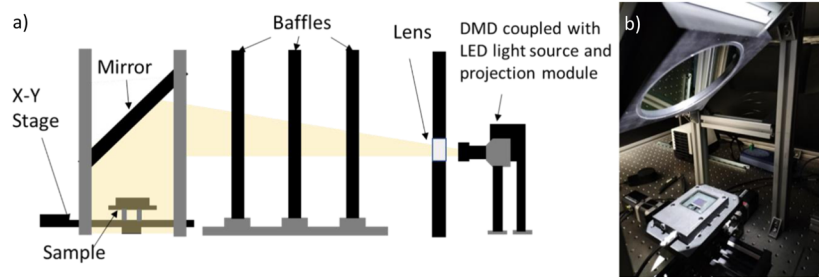


**FIG. 1.** (a) Schematic of our measurement system depicting how light is transferred from the LED onto the sample plane. (b) Light is reflected from a mirror held at a 45° angle onto the sample. A KG5 silicon reference cell is used to set the illuminance level of the DMD.

Patterns projected from the DMD were used to significantly improve the spatial uniformity of the ROI. Below, we describe the characterization and classification of the DLP system according to IEC TS 62607-7-2:2023.

#### IV. SYSTEM CLASSIFICATION

##### A. Indoor spectral coincidence

While IEC 60904-9 (classification of solar simulator characteristics)<sup>21</sup> considers the deviation of relative irradiance within spectral bands, this is not a suitable methodology for indoor spectral coincidence evaluation; the sharp spectral features of artificial light sources result in significant errors and deviations. Hence, IEC TS 62607-7-2:2023 proposes a different process to calculate the spectral coincidence of light sources.<sup>11</sup>

The spectral coincidence SC is defined by the worst-case value of the spectral mismatch between the reference spectrum and the measured spectrum,

$$SC = \frac{\int_{380}^{780} E_{\text{meas}}(\lambda) S_K(\lambda) d\lambda}{\int_{380}^{780} E_{\text{ref}}(\lambda) S_K(\lambda) d\lambda}, \quad (1)$$

where  $E_{\text{meas}}(\lambda)$  is the measured spectral profile of the light source,  $E_{\text{ref}}(\lambda)$  is the spectral profile of the reference spectrum (CIE LED-B4 in this case), and  $S_K(\lambda)$  ( $K = 1, \dots, 5$ ) is the spectral response of simulated IPV device number  $K$  labeled PV-1 to PV-5. These correspond to five different relative standard spectral responsivities of emerging IPV technologies, as listed in IEC TS 62607-7-2:2023 (spectral responsivity tables are also provided in the document).<sup>11</sup> The defined reference spectrum is the same at all illuminance levels under ISTCs and for measuring any IPV technology. The worst-case value is defined by the IPV device that has the largest deviation of the spectral coincidence from 1. As the reference spectrum is defined

within the wavelength range of 380–780 nm, the spectral mismatch between the measured IPV device and the reference is determined only within this band; any datapoints outside this range will yield zero values.

Figure 2(a) presents the normalized spectral profiles of the measured light output at the sample plane at the three different illuminance levels of 50, 200, and 1000 lx. The spectrum was measured at the sample plane using a calibrated Ocean-HDX spectrometer at the center of the sample plane. The CIE LED B4 reference spectrum is also included in the same graph and is defined for wavelengths of 380–780 nm. As can be observed, the spectral variations of the DLP system at different light levels are very low, calculated to be 0.2% in the worst case. The reported spectral variation is lower than using optical attenuation methods reported in the literature, and this enhances the benefit of digital light processing in our measurement system.<sup>12</sup>

The spectral coincidence values for these spectral profiles were calculated using Eq. (1) and the tabular data provided in IEC TS 62607-7-2:2023. Each simulated device has a bandgap that decreases from ~2.40 eV (PV-1) to ~1.12 eV (PV-5). Our light source has the worst spectral coincidence with PV-1, due to spectral deviations with our LED and the reference spectrum between 440 and 520 nm. The results of these calculations are presented in the right of Fig. 2(b); therefore, a spectral coincidence of 0.91 is reported for our DLP system.

In practice, when measuring IPV devices in our DLP system, a KG5 reference cell is used to set the light intensity, so spectral mismatch factors will be applied to each DUT to ensure all devices are measured at the same effective illuminance. This is similar to the process described in IEC 60904-7:2019<sup>22</sup> (computation of the spectral mismatch correction for measurements of photovoltaic devices). Our reference cell has been calibrated internally for linearity and spectral response, while its absolute spectral response data were used to calculate the expected short-circuit currents at 50, 200, and

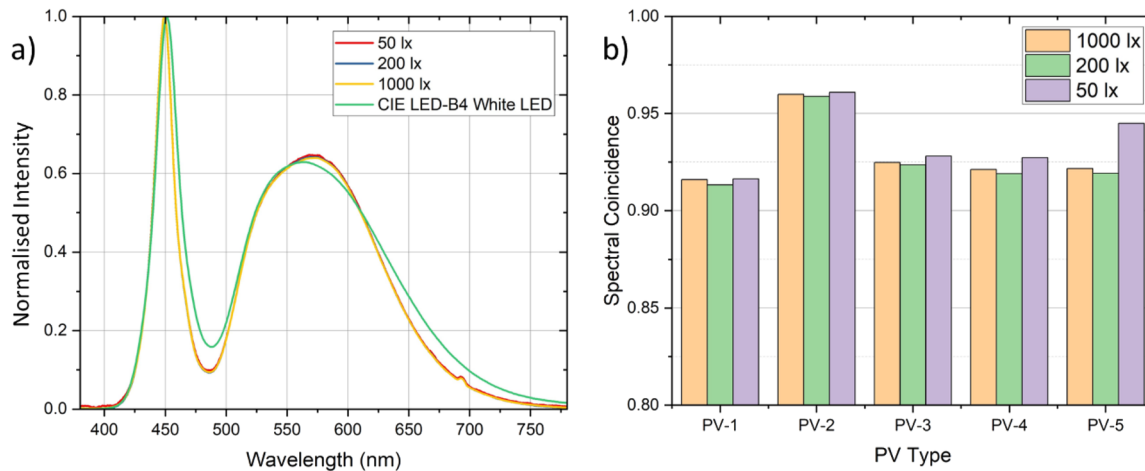


**FIG. 2.** (a) Normalized spectral profile of the measured spectrum of the light output of the system at the sample plane at the three required illuminance levels, 1000, 200, and 50 lx. The spectral variation between different light levels is lower than 0.2%. The reference spectrum of the CIE LED B4 spectrum is included in the same graph. (b) Spectral coincidence between the measured and reference spectrum for each of the simulated IPV devices in the IEC TS 62607-7-2:2023 tabular data. The spectral coincidence for the DLP system is calculated to be 0.91.

1000 lx. This is necessary since there are currently no reference cells available on the market for determining the irradiance at the sample plane for IPV testing. A significant advantage of our DLP system's feature of fine tuning the irradiance level while maintaining spectral profile and uniformity is that such spectral mismatch corrections of irradiance can be accurately and easily applied. This is important because spectral mismatches between DUTs and the reference cell used are expected, considering the variability in possible spectral response profiles of different IPV technologies.

## B. Non-uniformity

Uniform illumination of the measurement area is crucial for accurate measurements and low uncertainties; hence, illuminance non-uniformity is included in the light source classification. Illuminance non-uniformity (in %) is calculated as

$$NU_{ROI} = \frac{(L_{\max} - L_{\min})}{(L_{\max} + L_{\min})} \times 100, \quad (2)$$

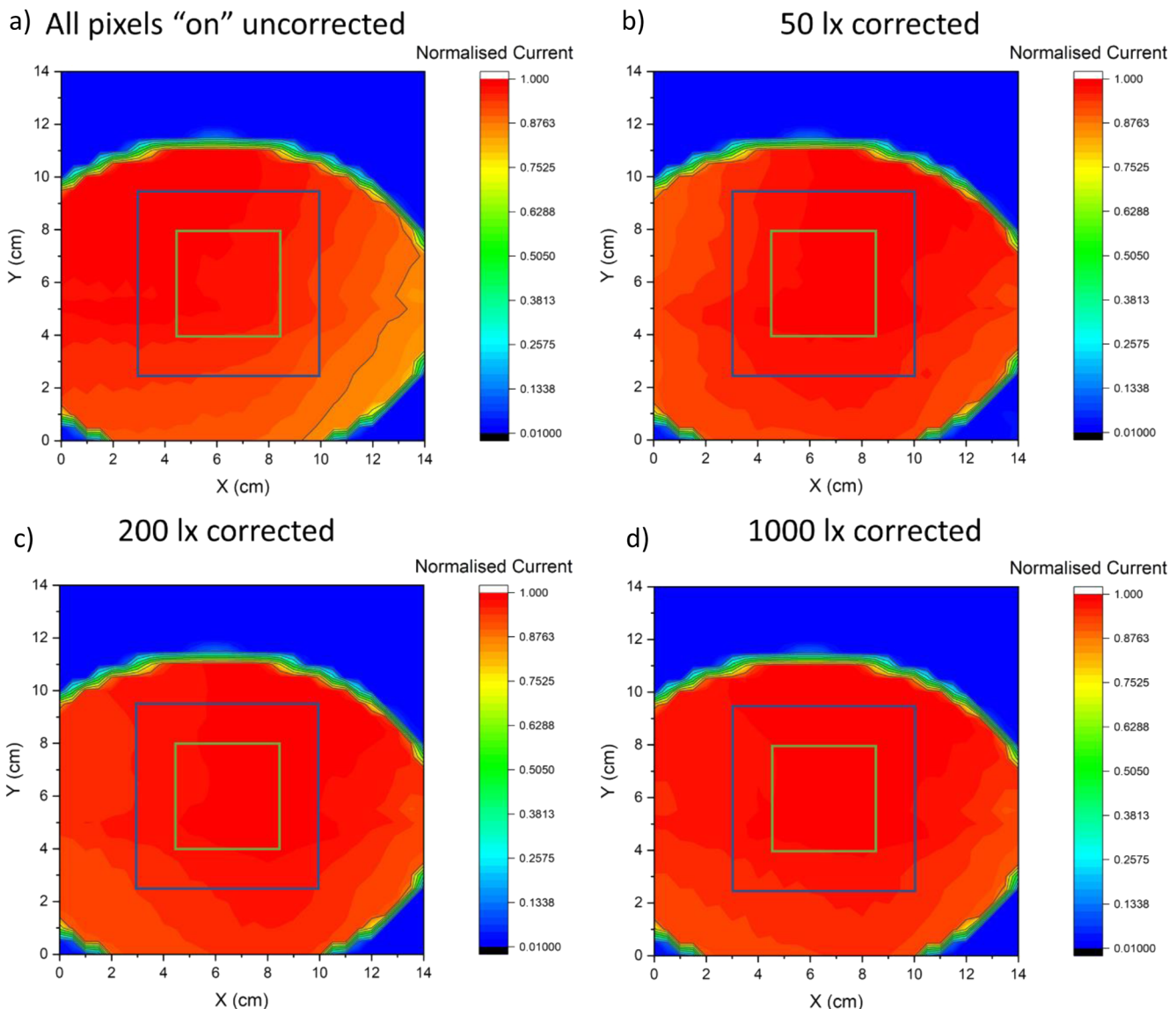


**FIG. 3.** Photocurrent maps of the spatial profile of light intensity at the sample plane of the DLP system: (a) All pixels are on, (b) illuminance of 1000 lx, (c) at 200 lx, and (d) at 50 lx. The photodiode has a 1 mm diameter pinhole aperture on top to minimize angular effects from the response of the photodiode and any divergence of the pseudo collimated light source.

where  $I_{\max}$  is the maximum illuminance in the ROI and  $I_{\min}$  is the minimum illuminance in the ROI. These can be measured using a stable PV device or photodiode. We used a calibrated Newport 818-UV photodiode without an attenuator, with a 1 mm diameter pinhole to remove indirect light, to determine the uniformity. The photodiode used is linear in the range of 50–1000 lx, which is a prerequisite for accurate uniformity evaluation at the different light levels; therefore, the photocurrent measured is directly proportional to the intensity of the incident light. Non-uniformity is thus calculated by,

$$NU_{ROI} = \frac{(I_{\max} - I_{\min})}{(I_{\max} + I_{\min})} \times 100, \quad (3)$$

where  $I_{\max}$  is the maximum measured photocurrent in the ROI and  $I_{\min}$  is the minimum measured photocurrent in the ROI. We performed a raster scan of the photodiode across the full illumination area and measured the photocurrent at each point. We used a calibrated KG5-filtered Si reference cell to determine the illuminance at the sample plane. The reference cell has been characterized in terms of linearity and spectral response, so that it is linear at this illuminance range, while its spectral response data were used to calculate the expected short-circuit currents at 50, 200, and 1000 lx. This is necessary since there are currently no reference cells available on the market for determining the irradiance at the sample plane for IPV testing.

There are significant benefits regarding uniformity of light intensity when using the DLP system: achieving the different irradiance levels at the sample plane without affecting uniformity and being able to correct for non-uniformity effects. Regarding light intensity, when all the pixels of the DLP systems are “on” (all micromirrors of the DMD are set in the “on” state), the illuminance at the sample plane can be much higher than 1000 lx at the typical operating current of the LED. In order to set appropriate illuminance values at the sample plane, DMD pixels are turned “off” to reduce the illuminance and meet the required ISTC values, as has also been demonstrated for linearity measurements with a similar system.<sup>14</sup>

A DMD can also be used for correcting optical non-uniformities on the sample plane. There are vignetting distortions from the projection optics of the DMD that cause major non-uniformities on the sample plane. As a DMD can be used to project binary patterns, spatial dithering is implemented to convert an image of the measured uniformity map into a binary image. The photocurrent of the projected area, when all pixels are “on,” is measured through the raster scan of a Newport 818-UV photodiode with a 1 mm pinhole, as presented in Fig. 3(a). The projection has been cropped as the whole light field is larger than the length of the measured area with the x-y stage; nevertheless, the edges are irrelevant as they are not used as active illumination areas in our system. A gradient is observed on the sample plane, which is due to both lens distortion effects from: the converging lens and the projection optics attached to the DMD. This photocurrent map can be used to model the flat-field correction function. By taking the inverse of this spatial function and applying the Floyd-Steinberg error matrix, we can create a spatially dithered binary image that removes flat-field distortions on our projection plane.<sup>23</sup> A non-linear least

**TABLE III.** Non-uniformity values for the different light levels, with an additional correction pattern applied.

Conditions area	All pixels “on”	1000 lx	200 lx	50 lx
$4 \times 4 \text{ cm}^2$	2.53%	1.69%	1.66%	1.51%
$7 \times 7 \text{ cm}^2$	5.4%	2.81%	3.07%	2.99%

squares fitting enables the creation of binary patterns for a range of illuminance levels by controlling the percentage of pixels in the image.

Results are shown in Fig. 3. The non-uniformity in Fig. 3(a) measured in the  $4 \times 4 \text{ cm}^2$  and  $7 \times 7 \text{ cm}^2$  ROIs, marked by the green and blue rectangles in each of the subplots, is 2.53% and 5.4%, respectively. Using the correction process and setting the illuminance at the required levels, at 1000 lx, the non-uniformity in the  $4 \times 4 \text{ cm}^2$  and  $7 \times 7 \text{ cm}^2$  ROIs in Fig. 3(b) has been reduced to 1.69% and 2.81%, respectively. Similar results are also reported for the measurements at 200 lx and 50 lx depicted in Figs. 3(c) and 3(d): non-uniformities at 200 lx were calculated to be 1.66% and 3.07% for the  $4 \times 4 \text{ cm}^2$  and  $7 \times 7 \text{ cm}^2$  ROI, respectively, while at 50 lx the same ROIs present non-uniformities of 1.51% and 2.99%. These uniformity optimization techniques can be potentially fine-tuned to further reduce non-uniformity values so that larger IPV devices can be measured under the same classification. The quoted non-uniformities at each illuminance are presented in Table III.

### C. Temporal stability

Temporal stability refers to fluctuations in the light source intensity at the sample plane during a measurement period. This is caused either by fluctuations in the current supply of an LED driver (or lamp driver in other cases), temperature fluctuations in the light source, or when LED boards or lamp bulbs are reaching the end of their lifetime. Fluctuations in LED driving current can also cause slight spectral shifts. Light source instabilities can affect the performance testing of IPV devices, leading to significant errors when performing an IV acquisition or setting the irradiance level with a reference cell. We used a KG5 filtered Si reference cell for the temporal stability measurements and placed it on the sample plane under constant illumination. This reference cell is linear; consequently, the variation in short-circuit current measured by a Keithley 2401B Sourcemeter is directly proportional to the fluctuation in light source intensity at the sample plane. The sample temperature during measurements was stable at 21 °C (at equilibrium with the lab temperature). Measurements were performed and presented here with all pixels “on” as a worst-case scenario of illumination to identify potential effects of system optics; however, appropriate measurements were also performed for all irradiance levels in the ISTCs.

Results are shown in Fig. 4, where the temporal short-circuit current ( $I_{SC}$ ) measurements of the reference cell are presented at 1 s intervals. Recording of measurements started as soon as the LED was turned on; hence, there is a decay in the  $I_{SC}$  measured as the

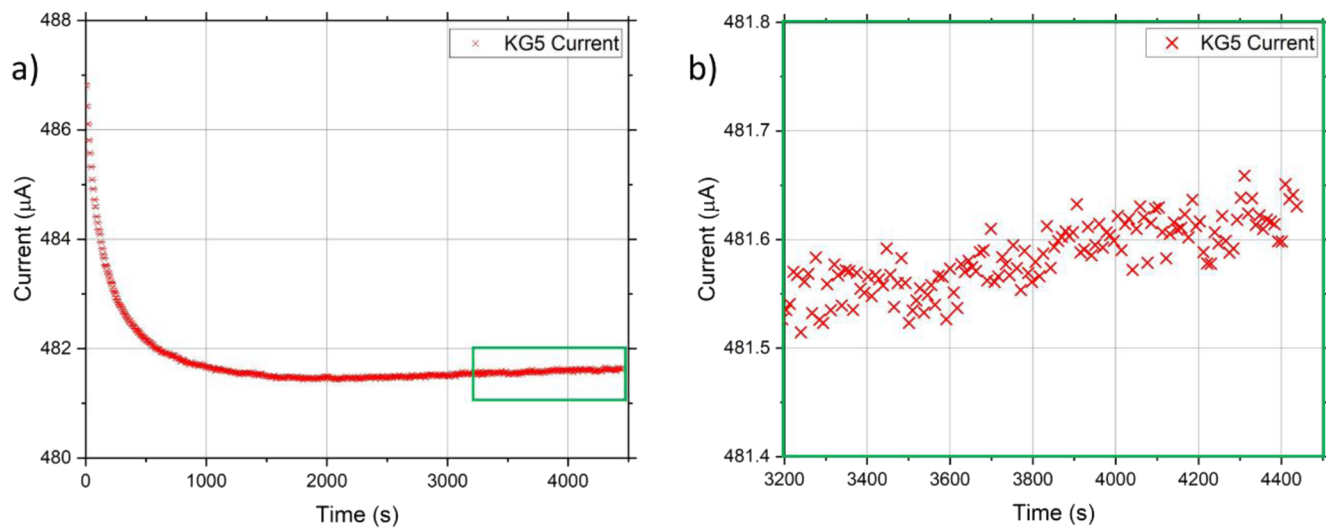


**FIG. 4.** (a)  $I_{SC}$  of the reference cell recorded with 1 s resolution for 75 min, with all pixels “on” for the DLP system. (b) Zoomed in graph to show the range of the fluctuations of  $I_{SC}$  recorded over 20 min of the measurement after the LED was stabilized.

LED thermally stabilizes. This was included to highlight that an initial thermal stabilization period should always be considered for an indoor light simulator. The LED is assumed to provide a stable output after  $\sim 1800$  s (30 min). In Fig. 4 (b), the  $I_{SC}$  over 20 min of the  $I_{SC}$  measurement after stabilization is presented. This specific length of time is chosen as this could be a representative amount of time required for I-V acquisition of an IPV device, including setting the irradiance levels, repeated I-V measurements, and considerations of sweep speeds for emerging technologies. The temporal stability (in %) is calculated by

$$TS = \frac{(I_{SC,max} - I_{SC,min})}{(I_{SC,max} + I_{SC,min})} \times 100, \quad (4)$$

where  $I_{SC,max}$  is the maximum short-circuit current measured in the identified measurement period and  $I_{SC,min}$  is the minimum short-circuit current recorded. The temporal stability is calculated from the relative deviation between the maximum and minimum  $I_{SC}$  measurements within the identified period (marked by the green box in Fig. 4), assuming an expected warm-up period of LED stabilization. Temporal stability includes short term stability (irradiance deviation between datapoints during acquisition) and long-term stability (irradiance stability from the start to the end of a set of measurements). In our case, long term stability will have the highest deviation, as can be observed in Fig. 4(b). The maximum and minimum reference  $I_{SC}$  values within Fig. 4(b) were found and substituted into Eq. (4) to determine the temporal stability of our measurement system as 0.015%.

#### D. Classification result and discussion

The results of the classification process according to IEC TS 62607-7-2:2023 for the DLP indoor light simulator system in this work are presented in Table IV. Potential improvements can be made to the system’s spectral coincidence and uniformity. This can

**TABLE IV.** Classification of the DLP system presented in this work based on IEC TS 62607-7-2:2023.

Classification parameter	Value	Class
Spectral coincidence	0.91	A
Non-uniformity	<1.69% for $4 \times 4 \text{ cm}^2$ area <2.99% for $7 \times 7 \text{ cm}^2$ area	SA
Temporal stability	<0.015%	SA

be achieved by using a different LED that is even closer to the CIE LED B4 reference spectrum and improving the projection optics and optical elements that deliver the pseudo-collimated light beam. Our spatial dithering algorithm can be further optimized by improving our flat-field correction model.

#### V. CONCLUSION

With the recent publication of the first edition of IEC TS 62607-7-2:2023, there is a need for the development of measurement systems that can deliver the defined specifications for accurate IPV performance testing. In this work, we present the first such system based on DLP technology to deliver the necessary system specifications. The use of DLP technology has enabled the delivery of a spectrally invariant light source across the necessary light intensity ranges for IPV testing. In addition, the use of spatial dithering and corrections using the DMD capabilities allows this system to achieve high uniformity illumination at the sample plane at all relevant irradiance levels.

Considering all classification parameters, spectral coincidence, non-uniformity, and temporal stability, the developed DLP system achieves classifications of A for a considered area of  $4 \times 4 \text{ cm}^2$  and B for larger areas up to  $7 \times 7 \text{ cm}^2$ . These specifications are achieved for

all illuminance levels of 50, 200, and 1000 lx. There is no significant variation in the spectral profile of the light source for the different light levels, something that is common when optical attenuators or LED current controls are used. The system delivers a pseudo-collimated beam rather than using diffuse illumination, resulting in lower uncertainties from angular response errors.

Standardization and harmonization activities are vital for emerging IPV technologies to become commercially available products within the near future. Through this work and the step-by-step description of the classification process based on IEC TS 62607-7-2:2023, more systems will be developed and become available, not only at research labs but also commercially, while more labs (academic, commercial, and industrial) will be able to develop their own equipment and at the same time evaluate it. A new market of indoor light simulator instruments for IPV device testing will be inevitably established, while this work has also highlighted the need for indoor PV reference cells, specifically calibrated at the irradiance levels defined in IEC TS 62607-7-2:2023, as with reference cells used at Standard Testing Conditions (STCs), to allow the proper implementation of these specifications. Considering the variability of indoor light conditions and types of illumination regarding spectra and directionality, the development of datasets and testing for energy rating of IPV devices can be considered similar to the IEC 61853 series [Photovoltaic (PV) module performance testing and energy rating: Parts 1–4].

As a result of this work, the development of further IPV device testing systems with different approaches and components will allow international intercomparison activities with multiple IPV device technologies. Such efforts will create the data and findings to feed back toward potential future revisions of IEC TS 62607-7-2:2023. Other complications that are not considered here and will be inevitably raised in the area of IPV testing are metastability effects during metastable IPV device testing, as such effects have been reported to have a significant impact on the power rating at STC.<sup>24,25</sup> Since perovskite and OPV devices are strong contenders for indoor light harvesting applications, such metastability effects should be considered in ISTC conditions as well by adopting appropriate measurement protocols.

## SUPPLEMENTARY MATERIAL

The supplementary material provided includes further information on the work presented in this paper. This material highlights the simulated spectral response curves in IEC TS 62607-7-2:2023, spectral deviations in altering LED forward current, and schematics of the DMD.

## ACKNOWLEDGMENTS

The work was co-funded by the UK Engineering and Physical Sciences Research Council (EPSRC) funded project “Application Targeted and Integrated Photovoltaics (ATIPs)” (Grant No. EP/T028513/1) and by the Department for Science, Innovation, and Technology (UK) through the National Measurement System. The authors would also like to acknowledge Dhaval Vankhade for providing feedback on this manuscript.

## AUTHOR DECLARATIONS

### Conflict of Interest

The authors have no conflicts to disclose.

### Author Contributions

**Daniel E. Parsons:** Conceptualization (equal); Data curation (lead); Formal analysis (lead); Investigation (equal); Methodology (equal); Resources (equal); Software (lead); Validation (supporting); Visualization (equal); Writing – original draft (equal); Writing – review & editing (supporting). **George Koutsourakis:** Conceptualization (equal); Formal analysis (equal); Funding acquisition (equal); Investigation (equal); Methodology (equal); Project administration (equal); Resources (equal); Supervision (equal); Validation (equal); Visualization (equal); Writing – original draft (equal); Writing – review & editing (equal). **James C. Blakesley:** Conceptualization (equal); Formal analysis (equal); Funding acquisition (equal); Investigation (equal); Methodology (equal); Project administration (equal); Resources (equal); Software (supporting); Supervision (equal); Validation (equal); Visualization (equal); Writing – review & editing (supporting).

## DATA AVAILABILITY

The data that support the findings of this study are available within the article.

## REFERENCES

- Mathews, S. N. Kantareddy, T. Buonassisi, and I. M. Peters, “Technology and market perspective for indoor photovoltaic cells,” *Joule* **3**(6), 1415–1426 (2019).
- V. Bahrami-Yekta and T. Tiedje, “Limiting efficiency of indoor silicon photovoltaic devices,” *Opt. Express* **26**(22), 28238 (2018).
- V. Pecunia, L. G. Occhipinti, and R. L. Z. Hoye, “Emerging indoor photovoltaic technologies for sustainable internet of things,” *Adv. Energy Mater.* **11**(29), 2100698 (2021).
- G. Burwell, O. J. Sandberg, W. Li, P. Meredith, M. Carnie, and A. Armin, “Scaling considerations for organic photovoltaics for indoor applications,” *Sol. RRL* **6**(7), 1–12 (2022).
- H. Michaels, M. Rinderle, R. Freitag, I. Benesperi, T. Edvinsson, R. Socher, A. Gagliardi, and M. Freitag, “Dye-sensitized solar cells under ambient light powering machine learning: Towards autonomous smart sensors for the internet of things,” *Chem. Sci.* **11**(11), 2895–2906 (2020).
- K.-L. Wang, Y.-H. Zhou, Y.-H. Lou, and Z.-K. Wang, “Perovskite indoor photovoltaics: Opportunity and challenges,” *Chem. Sci.* **12**(36), 11936–11954 (2021).
- H. K. H. Lee, J. Barbé, S. M. P. Meroni, T. Du, C.-T. Lin, A. Pockett, J. Troughton, S. M. Jain, F. De Rossi, J. Baker, M. J. Carnie, M. A. McLachlan, T. M. Watson, J. R. Durrant, and W. C. Tsui, “Outstanding indoor performance of perovskite photovoltaic cells—Effect of device architectures and interlayers,” *Sol. RRL* **3**(1), 1800207 (2019).
- B. Yan, X. Liu, W. Lu, M. Feng, H.-J. Yan, Z. Li, S. Liu, C. Wang, J.-S. Hu, and D.-J. Xue, “Indoor photovoltaics awaken the world’s first solar cells,” *Sci. Adv.* **8**(49), 1–9 (2022).
- D. Müller, E. Jiang, P. Rivas-Lazaro, C. Baretzky, G. Loukeris, S. Bogati, S. Paetel, S. J. C. Irvine, O. Oklobzija, S. Jones, D. Lamb, A. Richter, G. Siefer, D. Lackner, H. Helmers, C. Teixeira, D. Forgács, M. Freitag, D. Bradford, Z. Shen, B. Zimmermann, and U. Würfel, “Indoor photovoltaics for the internet-of-things—A

- comparison of state-of-the-art devices from different photovoltaic technologies,” *ACS Appl. Energy Mater.* **6**(20), 10404–10414 (2023).
- <sup>10</sup>T.-C. Wu, Y.-S. Long, S.-T. Hsu, and E.-Y. Wang, “Efficiency rating of various PV technologies under different indoor lighting conditions,” *Energy Procedia* **130**, 66–71 (2017).
- <sup>11</sup>International Electrotechnical Commission, IEC TS 62607-7-2 Part 7-2: Nano-Enabled Photovoltaics—Device Evaluation Method for Indoor Light (2023).
- <sup>12</sup>S. Zeiske, P. Meredith, A. Armin, and G. Burwell, “Importance of spectrally invariant broadband attenuation of light in indoor photovoltaic characterization,” *APL Energy* **1**(2), 026103 (2023).
- <sup>13</sup>L. J. Hornbeck, “The DMD<sup>TM</sup> projection display chip: A MEMS-based technology,” *MRS Bull.* **26**(4), 325–327 (2001).
- <sup>14</sup>G. Koutsourakis, T. Eales, I. Kroeger, and J. C. Blakesley, “High-resolution linearity measurements of photovoltaic devices using digital light processing projection,” *Meas. Sci. Technol.* **32**(5), 055901 (2021).
- <sup>15</sup>G. Koutsourakis, A. Thompson, and J. C. Blakesley, “Toward megapixel resolution compressed sensing current mapping of photovoltaic devices using digital light processing,” *Sol. RRL* **6**(5), 2100467 (2022).
- <sup>16</sup>T. Missbach, C. Karcher, and G. Siefer, “Frequency-division-multiplex-based quantum efficiency determination of solar cells,” *IEEE J. Photovoltaics* **6**(1), 266–271 (2016).
- <sup>17</sup>P. R. Michael, D. E. Johnston, and W. Moreno, “A conversion guide: Solar irradiance and lux illuminance,” *J. Meas. Eng.* **8**(4), 153–166 (2020).
- <sup>18</sup>A. S. Teran, J. Wong, W. Lim, G. Kim, Y. Lee, D. Blaauw, and J. D. Phillips, “AlGaAs photovoltaics for indoor energy harvesting in mm-scale wireless sensor nodes,” *IEEE Trans. Electron Devices* **62**(7), 2170–2175 (2015).
- <sup>19</sup>M. Bliss, T. Betts, R. Gottschalg, E. Salis, H. Müllejans, S. Winter, I. Kroeger, K. Bothe, D. Hinken, and J. Hohl-Ebinger, “Interlaboratory comparison of short-circuit current versus irradiance linearity measurements of photovoltaic devices,” *Sol. Energy* **182**, 256–263 (2019).
- <sup>20</sup>International Electrotechnical Commission, IEC 60904-1:2020 Photovoltaic Devices—Part 1: Measurement of Photovoltaic Current–Voltage Characteristics (2020).
- <sup>21</sup>International Electrotechnical Commission, IEC 60904-9:2020 Photovoltaic Devices—Part 9: Classification of Solar Simulator Characteristics (2020).
- <sup>22</sup>International Electrotechnical Commission, IEC 60904-7:2019 Photovoltaic Devices—Part 7: Computation of the Spectral Mismatch Correction for Measurements of Photovoltaic Devices (2019).
- <sup>23</sup>W. R. Floyd and L. Steinberg, “Adaptive algorithm for Spatial Grayscale,” *Proc. Soc. Inf. Disp.* **17**(2), 75–77 (1976).
- <sup>24</sup>T. Song, D. J. Friedman, and N. Kopidakis, “Comprehensive performance calibration guidance for perovskites and other emerging solar cells,” *Adv. Energy Mater.* **11**(23), 2100728 (2021).
- <sup>25</sup>G. Bardizza, H. Müllejans, D. Pavanello, and E. D. Dunlop, “Metastability in performance measurements of perovskite PV devices: A systematic approach,” *J. Phys. Energy* **3**(2), 021001 (2021).